Arabian Journal for Science and Engineering
https://doi.org/10.1007/s13369-024-08914-w

RESEARCH ARTICLE-CIVIL ENGINEERING

Static Response of Functionally Graded Porous Circular Plates via Finite Element Method

Silda Ghazi Mohammed Doori[1] · Ahmad Reshad Noori[1] · Ali Etemadi[2]

Received: 23 November 2023 / Accepted: 29 February 2024
© The Author(s) 2024

Abstract
The main purpose of this paper is to investigate the axisymmetric bending response of functionally graded porous (FGP) circular plates. The material properties are changed continuously in the thickness direction of the plate. Three distinct porosity distributions uniform, symmetric and monolithic are employed. The effect of porosity on the axisymmetric bending analysis of circular plates is examined parametrically. In this study, clamped and roller supports which commonly serve to achieve ideal boundary conditions in numerous engineering applications are used. The finite element method is employed for numerical analysis. The principal of the potential energy is used to obtain the governing equations. To generate the model of the FGP circular plates, an eight-node quadratic quadrilateral element with two degrees of freedom on each node is utilized. The results of this study are confirmed by the existing published literature. A good agreement between the results of the presented model and the previous literature has been observed. The results of the present study show that plate deflection increases with the increase of the porosity coefficient and the ratio of radius to thickness of circular plates. By increasing the porosity coefficient, the displacement values of the plates made of uniform porosity distribution is effected more than those of other porosity distributions.

Keywords Axisymmetric bending response · Finite element method · Circular plates · Porosity · Functionally graded porous materials

1 Introduction

Engineering applications may require a combination of various material properties. However, not all of these mechanical properties can be found in one material. If the materials are used together, it can cause large stress levels between the layers. One method to prevent such unfavorable consequences is to use functionally graded materials (FGMs). These material properties are gradually changing. By doing this, the structures' properties can be improved and the benefits of having multiple minerals in a single structure can be realized simultaneously. This kind of material has applications in high-temperature structures found in the nuclear, microelectronic and aerospace industries. In the field of processing techniques, successful examples of FGM were given [1]. Static analysis of FGM cylinders was done using a mesh-free method, and good results were obtained [2]. FGMs consist of two or more materials, and it is considered as an inhomogeneous material [3].

It seems that the material distributions and the strength of the FGM plates were significantly correlated. Research indicates that regulating the material's fracture behavior can lead to an increase in plate strength [4]. By applying a layer of FGM to the wire arc additive manufacturing process of laser metal deposition, the impact of bimetallic structures can be mitigated [5]. The analysis of FGM circular and rectangular plates were done using the FEM method [6]. Applications for composite materials have expanded significantly in recent years[7] because it is among the factors that lessen delamination and stress. The porous material

Ahmad Reshad Noori and Ali Etemadi have contributed equally.

✉ Silda Ghazi Mohammed Doori
eng.seldagazi@gmail.com

Ahmad Reshad Noori
arnoori@gelisim.edu.tr

Ali Etemadi
alietemadi@esenyurt.edu.tr

[1] Civil Engineering, Istanbul Gelisim University, Istanbul, Turkey

[2] Civil Engineering, Istanbul Esenyurt University, Istanbul, Turkey

Published online: 30 March 2024

appeared to have a positive effect on the design of sandwich plates, it both reduces the overall mass and increases the flexural strength [8]. It is possible to predict the stresses and deflections of 2D FG porous beams using the FEM approach [9]. On the other hand, the FGP material provides the structures with improved energy absorption, vibration reduction and thermal insulation capabilities [10]. Using the FEM approach, numerical static analysis of FGM plates were completed effectively [11–14]. Conversely, several studies use the FEM method to address the static response and buckling analysis of structural elements [15–18]. Additionally, the examination of FGM shells is one of the most prevalent subjects. It holds significance because of its extensive use in mechanical structures. When the numerical simulation results were compared to the literature, they demonstrated remarkable precision [19–21]. Several formulas and numerical solutions have been proposed to analyze heated FGM annular plates [22]. Conversely, research is being done on free vibration analysis for FGP plates [23]. Additionally, the researchers concentrated on examining the dynamic reactions and vibrations of FGP beams and plates [24–30]. The dynamic responses of axisymmetric circular plates have been successfully investigated [31]. The bending response of elliptic plates were examined by [32]. Numerous studies examine the stability analysis of FGM plates when they are loaded electromechanically [33]. Researchers [34] have been interested in the dynamic analysis of annular plates and solid circular and they examined effect of thickness functions and material variation exponents. FGM's nondeterministic structure verifies its responses to static loads in situations where the material's properties are uncertain [35]. A FEM-based ABAQUS tool is used to analyze the castellated beams' static response with different web opening sizes [36]. A parametric study is carried out to demonstrate how the natural frequencies and mode shapes of the structure are affected by various geometric parameters, boundary conditions, weight fraction of graphene platelets, porosity coefficient, distribution of porosity and graphene platelets' dispersion pattern. Furthermore, the natural frequency analyzed of a functionally graded porous joined truncated conical–cylindrical shell reinforced by graphene platelets [37]. Functionally graded (FG) porous rectangular plates' tendency to buckle under various loading scenarios was investigated in an alternate study [38]. Stress wave propagation and free vibration response of functionally graded graphene platelets of the shell are investigated under three different porosity distributions [39]. The performance of an axisymmetric rotating truncated cone subjected to a thermal loading composed of functionally graded (FG) porous materials is examined for (uniform and functionally graded), porosity distribution types [40]. The static response of functionally graded saturated porous rotating truncated cones was examined using three distinct patterns for the porosity distribution [41]. The low-velocity impact study results of the graphene platelet-reinforced circular plate (FG) demonstrate that the porosity distribution affects the structure's instantaneous central deflection and time history of contact force more than other parameters [42]. Static and transient responses of the plate based on Hamilton's principle for shear deformation plate theory using FEM was analyzed for different porosity coefficients [43]. Apart from the porosity coefficient, the natural frequency of FG is significantly influenced by the porosity distribution [44]. It has been found that a high weight fraction and a high porosity coefficient generate the strongest and lowest effects of FG on the buckling loads of the structure [45]. Three functions for porosity distribution were investigated in order to determine the optimal distribution of porosity for the torsional buckling forces of the shell [46].

The primary purpose of this paper is to suggest an efficient numerical method to examine the axisymmetric bending response of FGP circular plates. The FEM method is used to analyze the model for the numerical solution. The results obtained are compared with those of the available in the literature.

Literature review shows that there are several studies dealing with analyzing the static response of circular plates. Accordingly, the static response of uniform (UMCR), symmetric (SMCR) and monolithic (MMCR) functionally graded porous (FGP) circular plates is studied via the finite element method (FEM) by using eight-node quadratic quadrilateral axisymmetric element in this paper for the first time. The modulus of elasticity of the plate varies continually in the thickness direction. While the Poisson ratio (v) value is assumed to be constant. For verification, the static response of the FGM plate is examined for porosity coefficient ($e_0 = 0.2$, 0.4 and 0.9). Moreover, several examples of (h/r) are analyzed using different values of radius ($r = 1$–5 m), for various types of porosity coefficients (0.1–0.9). The clamped boundary condition is used for verification, while the clamped and roller-support types of boundary conditions are employed in the analysis of FGP plates. As a consequence, the FGP circular plate's deflection results show excellent agreement when compared to those obtained with the ANSYS APDL software. However, there is a great deal of agreement when comparing the FGM circular plate results with those reported in the literature that is currently in publication, including solutions derived using the complementary functions method (CFM).

2 Materials and Method

In this study, circular plates are subjected to the axisymmetric loading. Three-dimensional (3D) problems can be

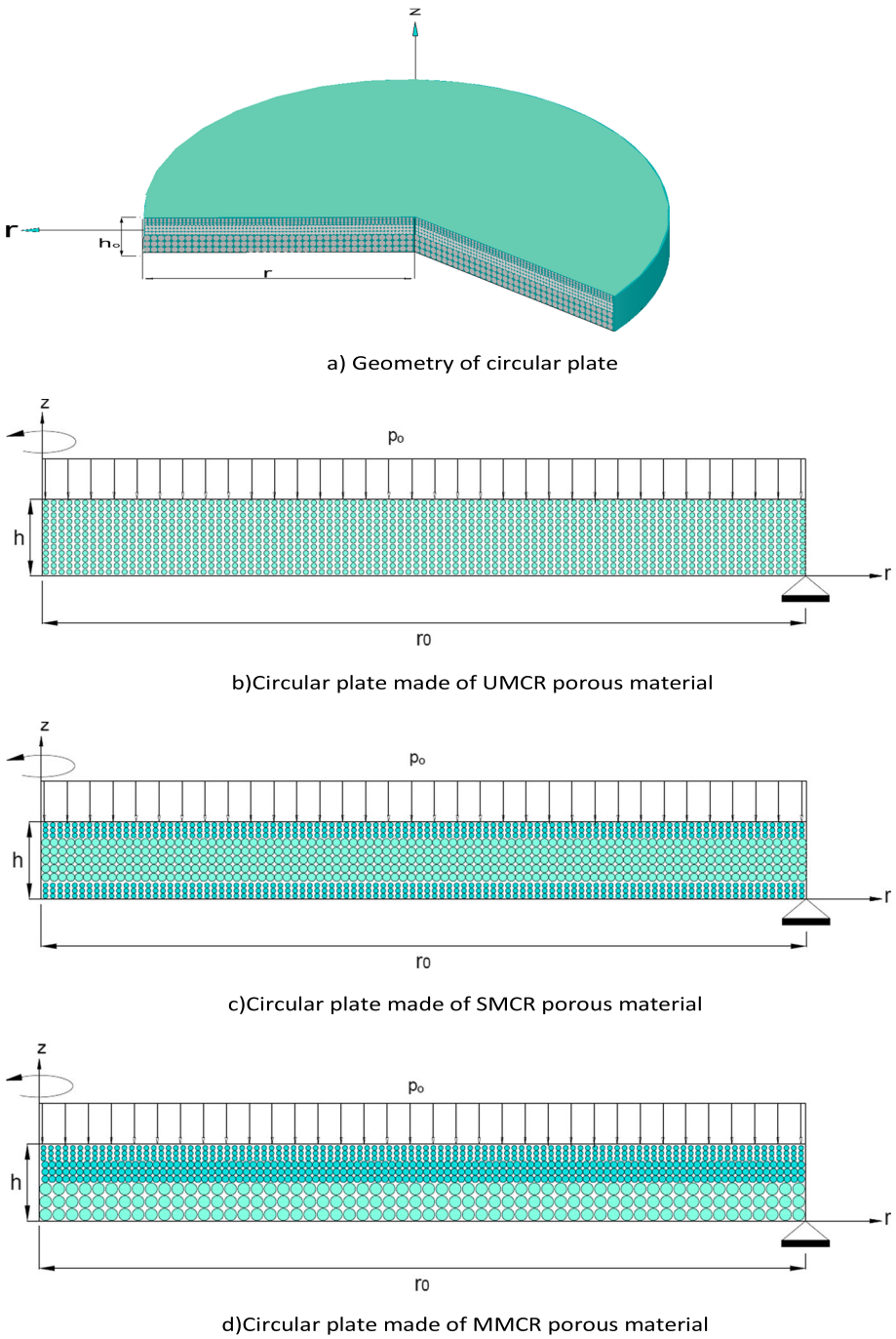


Fig. 1 Geometry of Circular plate with different porosity distributions

analyzed as simple two-dimensional (2D) problems. The problems are reviewed in the r-z plane. Three different material distributions are assumed in this study as shown in Fig. 1. The materials' mechanical properties are supposed to change along the thickness direction. Uniform porosity type (UMCR) is regularly distributed throughout the plate, whereas the effects of the SMCR type are assumed to be harmonic around the center of the plate. Regarding the monolithic MMCR type, the effects of porosity vary from highest to lowest ratio, along the thickness direction.

2.1 Stress and Strains Components

Considering the unit volume, the potential energy can be obtained as in Eqs. (1–2), which is dealing with the following parameters [47];

dA = area, dz = thickness direction, dr = radial direction, = $d\theta$ angular direction

$$\Pi = \frac{1}{2}\int_0^{2\pi}\int_A \boldsymbol{\sigma}^{\mathrm{T}}\boldsymbol{\varepsilon} r dA d\theta - \int_0^{2\pi}\int_A \mathbf{m}^{\mathrm{T}}\mathbf{f} r \mathrm{d}A d\theta - \int_0^{2\pi}\int_L \mathbf{m}^{\mathrm{T}}\mathbf{T} r \mathrm{d}l d\theta - \sum_i \mathbf{m}_i^{\mathrm{T}}\mathbf{P}_i \tag{1}$$

$$\Pi = 2\pi\left(\frac{1}{2}\int_A \boldsymbol{\sigma}^{\mathrm{T}}\boldsymbol{\varepsilon} r dA - \int_A \mathbf{m}^{\mathrm{T}}\mathbf{f} r \mathrm{d}A - \int_L \mathbf{m}^{\mathrm{T}}\mathbf{T} r \mathrm{d}l\right) - \sum_i \mathbf{m}_i^{\mathrm{T}}\mathbf{P}_i \tag{2}$$

The vertical (m) and horizontal (n) displacements of any point can be written as:

$$m = m(r, z),\ n = n(r, z) \tag{3}$$

The weight and distributed loads are given as:

$$\{\mathrm{f}\} = \{f_r, f_z\}^T,\ \{t\} = \{t_r, t_z\}^T$$

The relationship between the strain and displacement is given as follows: (4)

$$\{\varepsilon\} = \{\varepsilon_r, \varepsilon_z, \varepsilon_\theta, \gamma_{\mathrm{rz}}\}^{\mathrm{T}} = \left\{\frac{\partial \mathrm{m}}{\partial \mathrm{r}}, \frac{\partial \mathrm{n}}{\partial \mathrm{z}}, \frac{m}{\mathrm{r}}, \frac{\partial \mathrm{m}}{\partial \mathrm{z}} + \frac{\partial \mathrm{n}}{\partial \mathrm{r}}\right\} \tag{5}$$

The stress vector is as below:

$$\{\sigma\} = \{\sigma_r, \sigma_Z, \sigma_\theta, \tau_{\mathrm{rz}}\}^T \tag{6}$$

The constitutive relation is shown in Eq. (7).

$$\{\sigma\} = [C]\{\varepsilon\} \tag{7}$$

$$\begin{Bmatrix}\sigma_r\\ \sigma_z\\ \sigma_\theta\\ \tau_{\mathrm{rz}}\end{Bmatrix} = \begin{bmatrix}(1-\nu)p(z) & \nu p(z) & \nu p(z) & 0\\ & (1-\nu)p(z) & \nu p(z) & 0\\ & & (1-\nu)\mathrm{p}(z) & 0\\ \text{Symmetrical} & & & G(z)\end{bmatrix}\begin{Bmatrix}\varepsilon_r\\ \varepsilon_z\\ \varepsilon_\theta\\ \gamma_{\mathrm{rz}}\end{Bmatrix} \tag{8}$$

The Young's modulus E(z) and the shear modulus G(z) are defined by Eqs. (9–10).

$$p(z) = \frac{E(z)}{(1+\nu)(1-2\nu)} \tag{9}$$

$$G(z) = \frac{E(z)}{2(1+\nu)} \tag{10}$$

The porosity for SMCR, UMCR and MMCR models can be described by the relations in Eqs. (11–17) [48].

$$\begin{aligned}E(z) &= E_1\left[1-\cos\left(\frac{\pi z}{h}\right)\right] + E_0\cos\left(\frac{\pi z}{h}\right)\\ &= E_1\left[1-e_0\cos\left(\frac{\pi z}{h}\right)\right]\end{aligned} \tag{11}$$

$$\begin{aligned}G(z) &= G_1\left[1-\cos\left(\frac{\pi z}{h}\right)\right] + G_0\cos\left(\frac{\pi z}{h}\right)\\ &= G_1\left[1-e_0\cos\left(\frac{\pi z}{h}\right)\right]\end{aligned} \tag{12}$$

$$\begin{aligned}E(z) &= E_1\left[1-e_0\left(\frac{1}{e_o}-\frac{1}{e_o}\left(\frac{2}{\pi}\sqrt{1-e_o}-\frac{2}{\pi}+1\right)^2\right)\right]\\ &= E_1\left[1-e_0\psi\right]\end{aligned} \tag{13}$$

$$\begin{aligned}G(z) &= G_1\left[1-e_0\left(\frac{1}{e_o}-\frac{1}{e_o}\left(\frac{2}{\pi}\sqrt{1-e_o}-\frac{2}{\pi}+1\right)^2\right)\right]\\ &= G_1\left[1-e_0\psi\right]\end{aligned} \tag{14}$$

$$\psi = \frac{1}{e_o}-\frac{1}{e_o}\left(\frac{2}{\pi}\sqrt{1-e_o}-\frac{2}{\pi}+1\right)^2 \tag{15}$$

$$E(z) = E_1\left[1-e_0\cos\left(\frac{\pi z}{2h}+\frac{0.5\pi}{2}\right)\right] \tag{16}$$

$$G(z) = G_1\left[1-e_0\cos\left(\frac{\pi z}{2h}+\frac{0.5\pi}{2}\right)\right] \tag{17}$$

In these equations, e_0 is the porosity coefficient and h shows the thickness of the plate.

2.2 FEM Approach

As shown in Fig. 2, an isoparametric eight-node quadratic element is used in this study.

The coordinates of nodes can be obtained with the aid of Eq. (18), where, r_i and z_i are the coordinates of the node i,

$$r = \sum_{i=1}^{8} N_i r_i;\ z = \sum_{i=1}^{8} N_i z_i \tag{18}$$

N_i are the quadratic shape functions. Quadratic base polynomials with 8 parameters are chosen for displacements as:

$$m(\xi, \eta) = \{P(\xi, \eta)\}^T\{a\},\ n(\xi, \eta) = \{P(\xi, \eta)\}^T \tag{19}$$

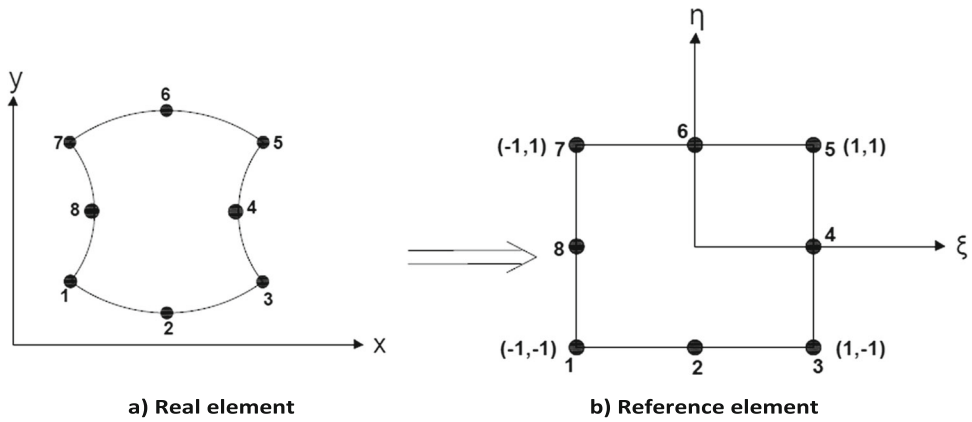


Fig. 2 Eight-node quadratic quadrilateral element

$$m = a_1 + \xi a_2 + \eta a_3 + \xi^2 a_4 + \xi\eta a_5 + \eta^2 a_6 + \xi^2\eta a_7 + \xi\eta^2 a_8 \tag{20}$$

$$n = a_1 + \xi a_2 + \eta a_3 + \xi^2 a_4 + \xi\eta a_5 + \eta^2 a_6 + \xi^2\eta a_7 + \xi\eta^2 a_8 \tag{21}$$

$$m(\xi_i, \eta_i) = m_i (i = 1, 2, \ldots, 8) \tag{22}$$

The m_i displacement for 8 nodes of the reference element is given in matrix form as follows:

$$\underbrace{\begin{Bmatrix} m_1 \\ m_2 \\ m_3 \\ m_4 \\ m_5 \\ m_6 \\ m_7 \\ m_8 \end{Bmatrix}}_{M_d} = \underbrace{\begin{bmatrix} 1 & \xi_1 & \eta_1 & \xi_1^2 & \xi_1\eta_1 & \eta_1^2 & \xi_1^2\eta_1 & \xi_1\eta_1^2 \\ 1 & \xi_2 & \eta_2 & \xi_2^2 & \xi_2\eta_2 & \eta_2^2 & \xi_2^2\eta_2 & \xi_2\eta_2^2 \\ 1 & \xi_3 & \eta_3 & \xi_3^2 & \xi_3\eta_3 & \eta_3^2 & \xi_3^2\eta_3 & \xi_3\eta_3^2 \\ 1 & \xi_4 & \eta_4 & \xi_4^2 & \xi_4\eta_4 & \eta_4^2 & \xi_4^2\eta_4 & \xi_4\eta_4^2 \\ 1 & \xi_5 & \eta_5 & \xi_5^2 & \xi_5\eta_5 & \eta_5^2 & \xi_5^2\eta_5 & \xi_5\eta_5^2 \\ 1 & \xi_6 & \eta_6 & \xi_6^2 & \xi_6\eta_6 & \eta_6^2 & \xi_6^2\eta_6 & \xi_6\eta_6^2 \\ 1 & \xi_7 & \eta_7 & \xi_7^2 & \xi_7\eta_7 & \eta_7^2 & \xi_7^2\eta_7 & \xi_7\eta_7^2 \\ 1 & \xi_8 & \eta_8 & \xi_8^2 & \xi_8\eta_8 & \eta_8^2 & \xi_8^2\eta_8 & \xi_8\eta_8^2 \end{bmatrix}}_{P} \underbrace{\begin{Bmatrix} a_1 \\ a_2 \\ a_3 \\ a_4 \\ a_5 \\ a_6 \\ a_7 \\ a_8 \end{Bmatrix}}_{a} \tag{23}$$

$$\{M_d\} = [P_d]\{a\} \tag{24}$$

$$[P_d]_{ij} = P_j(\xi_i, \eta_i), \{M_d\} = [P_d]\{a\}, \{a\} = [P_d]^{-1}\{M_d\} \tag{25}$$

$$m(\xi, \eta) = \underbrace{\{P(\xi, \eta)\}^T [P_d]^{-1}}_{\text{shape functions}} \{M_d\} \tag{26}$$

The shape functions are presented as:

$$\{\mathrm{N}(\xi, \eta)\}^{\mathrm{T}} = \{\mathrm{P}(\xi, \eta)\}^{\mathrm{T}}[\mathrm{P_d}]^{-1} \tag{27}$$

$$\{\mathrm{N}_1, \mathrm{N}_2, \mathrm{N}_3, \mathrm{N}_4, \mathrm{N}_5, \mathrm{N}_6, \mathrm{N}_7, \mathrm{N}_8\}^{\mathrm{T}} = \left\{1, \xi, \eta, \xi^2, \text{,}, \eta^2, \xi^2\eta, \xi\eta^2\right\}^{\mathrm{T}}[\mathrm{P_d}]^{-1} \tag{28}$$

The shape functions obtained by multiplying the matrices from Eq. (28) are given in Eqs. (29–36) [49]:

$$\mathrm{N}_1 = \frac{1}{4}(-1+\xi)(1-\eta)(1+\xi+\eta) \tag{29}$$

$$N_2 = \frac{1}{2}\left(-1+\xi^2\right)(-1+\eta) \tag{30}$$

$$N_3 = \frac{1}{4}(1+\xi)(-1+\eta)(1-\xi+\eta) \tag{31}$$

$$N_4 = \frac{1}{2}(1+\xi)\left(1-\eta^2\right) \tag{32}$$

$$N_5 = \frac{1}{4}(1+\xi)(1+\eta)(-1+\xi+\eta) \tag{33}$$

$$N_6 = \frac{1}{2}\left(1-\xi^2\right)(1+\eta) \tag{34}$$

$$N_7 = \frac{1}{4}(-1+\xi)(1+\eta)(1+\xi-\eta) \tag{35}$$

$$N_8 = \frac{1}{2}(-1+\xi)\left(-1+\eta^2\right) \tag{36}$$

The vertical and horizontal displacements at any point of the element also depend on the shape functions.

$$m = \sum_{\mathrm{i}=1}^{8} N_{\mathrm{i}} m_{\mathrm{i}};\ n = \sum_{\mathrm{i}=1}^{8} N_{\mathrm{i}} n_{\mathrm{i}} \tag{37}$$

2.3 Element Stiffness Matrix

Strain and displacements relations are given [47]:

$$\begin{Bmatrix} \varepsilon_r \\ \varepsilon_z \\ \varepsilon_\theta \\ \gamma_{rz} \end{Bmatrix} = \begin{bmatrix} \frac{\partial}{\partial \mathrm{r}} & 0 \\ 0 & \frac{\partial}{\partial \mathrm{Z}} \\ \frac{1}{\mathrm{r}} & 0 \\ \frac{\partial}{\partial \mathrm{Z}} & \frac{\partial}{\partial \mathrm{r}} \end{bmatrix} \begin{Bmatrix} m \\ n \end{Bmatrix} \tag{38}$$

$$\{\varepsilon\} = \sum_{\mathrm{i}=1}^{8} \begin{bmatrix} \frac{\partial N_\mathrm{i}}{\partial r} & 0 \\ 0 & \frac{\partial N_\mathrm{i}}{\partial z} \\ \frac{N_\mathrm{i}}{r} & 0 \\ \frac{\partial N_\mathrm{i}}{\partial \mathrm{Z}} & \frac{\partial N_\mathrm{i}}{\partial \mathrm{r}} \end{bmatrix} \begin{Bmatrix} m_\mathrm{i} \\ n_\mathrm{i} \end{Bmatrix} = \sum_{\mathrm{i}=1}^{8} [B_\mathrm{i}]\{\mathrm{d_i}\} \tag{39}$$

$$[B_\mathrm{i}] = \begin{bmatrix} \frac{\partial N_\mathrm{i}}{\partial \mathrm{r}} & 0 \\ 0 & \frac{\partial N_\mathrm{i}}{\partial z} \\ \frac{N_\mathrm{i}}{\mathrm{r}} & 0 \\ \frac{\partial N_\mathrm{i}}{\partial \mathrm{Z}} & \frac{\partial N_\mathrm{i}}{\partial \mathrm{r}} \end{bmatrix}; \{\mathrm{d_i}\} = \begin{Bmatrix} m_\mathrm{i} \\ n_\mathrm{i} \end{Bmatrix} \tag{40}$$

For all element

$$[B_\mathrm{i}] = \begin{bmatrix} \frac{\partial}{\partial \mathrm{r}} & 0 \\ 0 & \frac{\partial}{\partial \mathrm{Z}} \\ \frac{1}{\mathrm{r}} & 0 \\ \frac{\partial}{\partial \mathrm{Z}} & \frac{\partial}{\partial \mathrm{r}} \end{bmatrix} \begin{bmatrix} N_1 & 0 & N_2 & 0 & \cdots & N_8 & 0 \\ 0 & N_1 & 0 & N_2 & \cdots & 0 & N_8 \end{bmatrix} \tag{41}$$

$$\{d_e\}^t = \{m_1, n_1, m_2, n_2, m_3, n_3, m_4, n_4, m_5, n_5, m_6, n_6, m_7, n_7, m_8, n_8\} \tag{42}$$

$$\frac{\partial N_i}{\partial \xi} = \frac{\partial N_i}{\partial r}\frac{\partial r}{\partial \xi} + \frac{\partial N_i}{\partial z}\frac{\partial z}{\partial \xi} \tag{43}$$

$$\frac{\partial N_i}{\partial \eta} = \frac{\partial N_i}{\partial r}\frac{\partial r}{\partial \eta} + \frac{\partial N_i}{\partial z}\frac{\partial z}{\partial \eta} \tag{44}$$

$$\begin{bmatrix} \frac{\partial N_i}{\partial \xi} \\ \frac{\partial N_i}{\partial \eta} \end{bmatrix} = \begin{bmatrix} \frac{\partial r}{\partial \xi} & \frac{\partial z}{\partial \xi} \\ \frac{\partial r}{\partial \eta} & \frac{\partial z}{\partial \eta} \end{bmatrix} \begin{bmatrix} \frac{\partial N_i}{\partial r} \\ \frac{\partial N_i}{\partial z} \end{bmatrix} = [J] \begin{bmatrix} \frac{\partial N_i}{\partial r} \\ \frac{\partial N_i}{\partial z} \end{bmatrix} \tag{45}$$

The Jacobian transformation is given as following Eq.:

$$[J] = \begin{bmatrix} \frac{\partial r}{\partial \xi} & \frac{\partial z}{\partial \xi} \\ \frac{\partial r}{\partial \eta} & \frac{\partial z}{\partial \eta} \end{bmatrix} = \begin{bmatrix} \sum_{i=1}^{8} \frac{\partial N_i}{\partial \xi} r_i & \sum_{i=1}^{8} \frac{\partial N_i}{\partial \xi} z_i \\ \sum_{i=1}^{8} \frac{\partial N_i}{\partial \eta} r_i & \sum_{i=1}^{8} \frac{\partial N_i}{\partial \eta} z_i \end{bmatrix} \tag{46}$$

$$\begin{bmatrix} \frac{\partial N_i}{\partial r} \\ \frac{\partial N_i}{\partial z} \end{bmatrix} = [J]^{-1} \begin{bmatrix} \frac{\partial N_i}{\partial \xi} \\ \frac{\partial N_i}{\partial \eta} \end{bmatrix} = \underbrace{\frac{1}{\det[J]} \begin{bmatrix} \frac{\partial z}{\partial \eta} & -\frac{\partial z}{\partial \xi} \\ -\frac{\partial r}{\partial \eta} & \frac{\partial r}{\partial \xi} \end{bmatrix}}_{[J]^{-1}=[J^*]} \begin{bmatrix} \frac{\partial N_i}{\partial \xi} \\ \frac{\partial N_i}{\partial \eta} \end{bmatrix} \tag{47}$$

$$\frac{\partial N_i}{\partial r} = J_{11}^* \frac{\partial N_i}{\partial \xi} + J_{12}^* \frac{\partial N_i}{\partial \eta} \tag{48}$$

$$\frac{\partial N_i}{\partial z} = J_{21}^* \frac{\partial N_i}{\partial \xi} + J_{22}^* \frac{\partial N_i}{\partial \eta} \tag{49}$$

The strain matrix [B] is calculated based on the reference element coordinates as follows:

$$[B_i] = \begin{bmatrix} J_{11}^* & J_{12}^* & 0 & 0 & 0 \\ 0 & 0 & J_{21}^* & J_{22}^* & 0 \\ 0 & 0 & 0 & 0 & 1/r \\ J_{21}^* & J_{22}^* & J_{11}^* & J_{12}^* & 0 \end{bmatrix} \begin{bmatrix} \frac{\partial N_i}{\partial \xi} & 0 \\ \frac{\partial N_i}{\partial \eta} & 0 \\ 0 & \frac{\partial N_i}{\partial \xi} \\ 0 & \frac{\partial N_i}{\partial \eta} \\ N_i & 0 \end{bmatrix} \tag{50}$$

Element stiffness matrix is given as following:

$$[k_e] = \iint_{A_e} \left\{ \int_0^{2\pi} [B]^T [C][B] r d\theta \right\} dr dz \tag{51}$$

$$dA = dr dz = \det[J] d\xi d\eta \tag{52}$$

If the element stiffness matrix is integrated over θ (0-2π), it becomes as follow:

$$[k_e] = 2\pi \int_{-1}^{+1} \int_{-1}^{+1} [B]^T [C][B] r \det[J] d\xi d\eta \tag{53}$$

$$\{f_h\} = \iint_{A_e} \left\{ \int_0^{2\pi} \{N\}^T \{f\} r d\theta \right\} dr dz \tag{54}$$

$$\{f_e\} = \rho g 2\pi \int_{-1}^{+1} \int_{-1}^{+1} \{N\}^T \{f\} r \det[J] d\xi d\eta \tag{55}$$

$$\{f_e\} = \int_{L_e} \left\{ \int_0^{2\pi} \{N\}^T \{T\} r d\theta \right\} dl \tag{56}$$

$$\{f_e\} = \int_{L_e} \left\{ \int_0^{2\pi} \{N\}^T \{T\} r d\theta \right\} \mathrm{d}l \tag{57}$$

$$\{f_e\} = 2\pi \int_{-1}^{+1} \{N\}^T \{T\} r \frac{L_e}{2} d\xi \tag{58}$$

The node load vector for the volume forces and the distributed forces acting on the element boundary is also obtained as follows:

Table 1 Boundary condition

Boundary condition	Symmetric condition	Support
Clamped	Ur = 0	Ur = 0
		Uz = 0
Roller supported	Ur = 0	Uz = 0

$$\{f_e\} = \rho(r)g2\pi \int_{-1}^{+1}\int_{-1}^{+1} \{N\}^T\{f\}r\det[J]d\xi d\eta + 2\pi \int_{-1}^{+1} \{N\}^T\{T\}r\frac{L_e}{2}d\xi \tag{59}$$

Two types of boundary conditions are used in this study and are presented in Table 1.

3 Numerical Results and Discussion

First of all, the numerical results of FGM circular plates for two types of boundary conditions and three different material distribution constants (0, 2 and 6), using the FEM are presented in this paper. For this purpose, computer program is coded in Fortran. To validate the chosen technique, the maximum values of the non-dimensional vertical displacements are compared with the available literature and those of the ANSYS (PLANE183) in Table 2. The modulus of elasticity of the plate varies continuously in thickness directions, while the Poisson ratio (v) is supposed to be constant (v = 0.288). Considering the plate is made of aluminum/zirconia. E_r depicts the ratio of the modulus of elasticity of aluminum and zirconia as in [50–52], which is equal to (E_r = 0.396). The E_m describes the modulus of elasticity of aluminum which is equal to (E_m = 70 Gpa), while the E_c describes the modulus of elasticity of zirconia. A circular plate subjected to a uniformly distributed load is considered. Radius of this plate, r_0 = 1.00 m, thickness, t = 0.10 m and load, p_z = 10 N/m^2. Equation 62 shows the maximum non-dimensional deflection ($\overline{w}$) and Dc refers to the flexural rigidity.

The result obtained for clamped and roller-supported boundary conditions is applicable to this study.

$$E(z) = (E_m - E_c)\left(\frac{h-2z}{2h}\right)^n + E_c \tag{60}$$

$$E_r = E_m/E_c \tag{61}$$

$$D_c = \frac{E_c h^3}{12(1-v^2)};\ \overline{w} = \frac{64Dc}{P_Z {r_0}^4 w_{max}} \tag{62}$$

Reddy et al. [51] used the analytics method, which depended on the first-order shear deformation (Mindlin plate) theory. Saidi et al. [50] used the closed-form method to employ the solutions based on the unconstrained third-order shear deformation plate theory (UTST), While Noori and Temel [52] used the CFM. It can be seen from Table 2 that the results of the presented approach are in excellent agreement with those of the previous literature. The main purpose of this paper is to investigate the porosity effects and the material properties, which is accepted to be changed in the thickness direction. For the design of the models, the uniform (UMCR) models, symmetric (SMCR)) and monolithic (MMCR) porosity material types are used. The plate is divided into 80 layers in the thickness direction. Taking into consideration, the thickness value of (h) is constant, which is equal to (h = 0.1 m), while the radius value is assumed to vary which is between (1–5 m). Poisson ratio (v) is taking constant with a value equal to (v = 0.3). Moreover, the plate is divided into 30 layers in the radial direction. As a result, the model of the plate consists of 2400 elements. To verify the results, the maximum vertical displacement values obtained from this study for porosity coefficient (e_0 = 0.2, 0.4 and 0.9) compared with ANSYS program, which is presented in Table 3, 4, 5, 6 and 7, respectively. Regarding the model in ANSYS, through the thickness of the plate, 80 layers of isotropic materials are defined and PLANE-183 element is used for the model. The plate is divided into 2400 elements. This solid element is defined by a quadratic 8-node element with two degrees of freedom at each node and translations in the nodal x and y directions with a torsion option for

Table 2 Verification of the FGM plate results for clamped type (mm)

Supported type	n	Ref. [50]	Ref. [51]	Ref. [52]	ANSYS (SHELL209)	ANSYS (PLANE183)	Present study
Clamped	0	2.6382	2.6390	2.6387	2.6386	2.628352	2.62610
	2	1.4429	1.4440	1.4469	1.4458	1.4369	1.44290
	6	1.2552	1.2570	1.2592	1.2581	1.2532	1.25899
Roller Supported	0	10.4810	10.4810	10.4812	10.4803	10.4556	10.45759
	2	5.7546	5.7560	5.7265	5.7611	5.7692	5.77197
	6	5.0058	5.0070	4.9847	5.0127	5.0313	5.03537

Table 3 Verification of the results with those of ANSYS for (h/r= 1/10) clamped circular plate (mm)

e_0	UMCR		MMCR		SMCR	
	ANSYS(PLANE183)	Present Study	ANSYS(PLANE183)	Present study	ANSYS(PLANE183)	Present study
0.2	0.0000097	0.0000097	0.000009143	0.00000996	0.009157000	0.00912457
0.4	0.0000115	0.0000115	0.000010008	0.00001089	0.000010009	0.00000993
0.9	0.0000265	0.0000265	0.000013684	0.00001487	0.000013798	0.00001348

Table 4 Verification of the results with those of ANSYS for (h/r = 1/20) clamped circular plate (mm)

e_0	UMCR		MMCR		SMCR	
	ANSYS(PLANE183)	Present Study	ANSYS(PLANE183)	Present study	ANSYS(PLANE183)	Present study
0.2	0.00015051	0.00015054	0.0001420	0.00015565	0.1414600	0.14095500
0.4	0.00017852	0.00017855	0.0001550	0.00017023	0.1538500	0.15263200
0.9	0.00041069	0.00041076	0.0002120	0.00023267	0.2001900	0.19553400

Table 5 Verification of the results with those of ANSYS for (h/r = 1/30) clamped circular plate (mm)

e_0	UMCR		MMCR		SMCR	
	ANSYS(PLANE183)	Present Study	ANSYS(PLANE183)	Present study	ANSYS(PLANE183)	Present study
0.2	0.00075733	0.000757593	0.00071296	0.00078448	0.7113300	0.70889700
0.4	0.00089825	0.000898556	0.00078050	0.00085796	0.7729200	0.76687500
0.9	0.00206640	0.00206715	0.00106940	0.00117297	0.9938500	0.97086500

Table 6 Verification of the results with those of ANSYS for (h/r = 1/40) clamped circular plate (mm)

e_0	UMCR		MMCR		SMCR	
	ANSYS(PLANE183)	Present study	ANSYS(PLANE183)	Present study	ANSYS(PLANE183)	Present study
0.2	0.0023888	0.00238934	0.00224890	0.00270732	2.243200	2.2352600
0.4	0.0028333	0.00283392	0.00246190	0.00270732	2.436600	2.4172400
0.9	0.0065182	0.00651951	0.00337370	0.00370166	3.119800	3.0472700

Table 7 Verification of the results with those of ANSYS for (h/r = 1/50) clamped circular plate (mm)

e_0	UMCR		MMCR		SMCR	
	ANSYS(PLANE183)	Present study	ANSYS(PLANE183)	Present Study	ANSYS(PLANE183)	Present study
0.2	0.0058267	0.00582759	0.0054852	0.00603902	5.4710000	5.4512200
0.4	0.0069108	0.00691190	0.0060050	0.00660473	5.9417000	5.8940800
0.9	0.0158990	0.01590110	0.0082294	0.00903085	7.5925000	7.4156400

Table 8 Maximum vertical displacement values of fixed supported UMCR porous circular plate (mm)

	h/r				
e_0	1/10	1/20	1/30	1/40	1/50
0.1	0.00000900	0.00014000	0.00070450	0.00222180	0.00541890
0.2	0.00000970	0.00015050	0.00075760	0.00238930	0.00582760
0.3	0.00001050	0.00016320	0.00082110	0.00258950	0.00631580
0.4	0.00001150	0.00017860	0.00089860	0.00283390	0.00691190
0.5	0.00001280	0.00019790	0.00099590	0.00314120	0.00766130
0.6	0.00001440	0.00022320	0.00112340	0.00354300	0.00864130
0.7	0.00001670	0.00025830	0.00130000	0.00410010	0.01000020
0.8	0.00002010	0.00031190	0.00156940	0.00494970	0.01207230
0.9	0.00002650	0.00041080	0.00206720	0.00651950	0.01590110

Table 9 Maximum vertical displacement values of fixed supported SMCR porous circular plate (mm)

	h/r				
e_0	1/10	1/20	1/30	1/40	1/50
0.1	0.00000877	0.00013578	0.00068312	0.00215426	0.00525398
0.2	0.00000912	0.00014096	0.00070890	0.00223526	0.00545122
0.3	0.00000951	0.00014655	0.00073672	0.00232265	0.00566394
0.4	0.00000993	0.00015263	0.00076688	0.00241724	0.00589408
0.5	0.00001040	0.00015928	0.00079968	0.00252002	0.00614396
0.6	0.00001093	0.00016659	0.00083558	0.00263218	0.00641638
0.7	0.00001155	0.00017474	0.00087514	0.00275534	0.00671493
0.8	0.00001233	0.00018405	0.00091936	0.00289188	0.00704464
0.9	0.00001348	0.00019553	0.00097087	0.00304727	0.00741564

the axisymmetric. For more information about this element, check the Mechanical APDL Element Reference [53].

The results obtained from the Tables 3, 4, 5, 6 and 7 have been examined for the clamped type of boundary condition. In this study, a computer program is coded in FORTRAN. The modulus of elasticity of the plate varies continually in the thickness direction, where ($E_1 = 210 \times 10^9$ N/m^2). To verify the results, several examples of (*h/r*) are analyzed. According to Tables 3, 4, 5, 6 and 7, the deflection of the plate increases as the porosity coefficient and (*h/r*) increase. For clamped circular plates, excellent agreement is observed between present study and the result of the ANSYS in the UMCR type, compared with the other two types. For MMCR, the largest difference between the ANSYS and the present study is observed in Table 7 for ($h/r = 1/50$) at porosity coefficients (0.9), while the biggest difference in SMCR type is seen in Table 3 for $h/r = 1/10$ at porosity coefficients 0.4.

As shown in Tables 8, 9, 10, 11, 12 and 13, the maximum deflection values are examined for two types of boundary conditions (clamped and roller supported), for various types of porosity coefficients (0.1–0.9) taking into consideration the different *h/r* values ($r = 1$–5 m).

The results show that when the value of the property coefficient (e_0) increases, so does the value of the maximum deflection for all types of porosity distribution increases. In addition, that when the value of (*h/r*) increases, the value of maximum deflection increases for all types of porosity distribution. Also, in Tables 8, 9, 10, 11, 12 and 13, for all types of boundary conditions. It is observed, that the highest value of maximum vertical displacement is recorded by roller-supported type in Table 11 for UMCR of porosity coefficient 0.9, *h/r* (1/50) and the lower value is recorded by clamped type in Table 9 for SMCR of porosity 0.1, *h/r* (1/10).

As for the clamped circular plate, the highest value of the maximum vertical displacement is observed in Table 8 for UMCR with porosity coefficient (0.9), while the lowest value is seen in Table 9 for (SMCR) type with the porosity coefficient (0.1). Regarding the roller-supported type, the highest value of maximum vertical displacement is recorded by the UMCR porous type in Table 11, while the lowest value is observed for SMCR porous type in Table 12.

As shown in Figs. 3, 4, 5, 6 and 7, a comparison of the maximum vertical displacement of the FGP circular plate for two types of boundary conditions is presented: clamped

Table 10 Maximum vertical displacement values of fixed supported MMCR porous circular plate (mm)

	h/r				
e_0	1/10	1/20	1/30	1/40	1/50
0.1	0.00000957	0.00014952	0.00075361	0.00237802	0.00580134
0.2	0.00000996	0.00015565	0.00078448	0.00247544	0.00603902
0.3	0.00001040	0.00016250	0.00081901	0.00258439	0.00630480
0.4	0.00001089	0.00017023	0.00085796	0.00270732	0.00660473
0.5	0.00001146	0.00017904	0.00090239	0.00284753	0.00694680
0.6	0.00001210	0.00018921	0.00095370	0.00300949	0.00734195
0.7	0.00001286	0.00020113	0.00101383	0.00319927	0.00780498
0.8	0.00001377	0.00021535	0.00108557	0.00342574	0.00835759
0.9	0.00001487	0.00023267	0.00117297	0.00370166	0.00903085

Table 11 Maximum vertical displacement values of roller-supported UMCR porous circular plate (mm)

	h/r				
e_0	1/10	1/20	1/30	1/40	1/50
0.1	0.00003570	0.00056760	0.00286970	0.00906540	0.02212770
0.2	0.00003840	0.00061040	0.00308610	0.00974920	0.02379680
0.3	0.00004160	0.00066150	0.00334460	0.01056590	0.02579030
0.4	0.00004560	0.00072390	0.00366030	0.01156320	0.02822450
0.5	0.00005050	0.00080240	0.00405720	0.01281680	0.03128440
0.6	0.00005700	0.00090510	0.00457620	0.01445650	0.03528610
0.7	0.00006590	0.00104740	0.00529580	0.01672980	0.04083560
0.8	0.00007960	0.00126440	0.00639310	0.02019640	0.04929670
0.9	0.00010480	0.00166550	0.00842070	0.02660150	0.06493180

Table 12 Maximum vertical displacement values of roller-supported SMCR porous circular plate (mm)

	h/r				
e_0	1/10	1/20	1/30	1/40	1/50
0.1	0.00003464	0.00055032	0.00278226	0.00878913	0.02145300
0.2	0.00003596	0.00057101	0.00288662	0.00911850	0.02225660
0.3	0.00003739	0.00059334	0.00299914	0.00947357	0.02312280
0.4	0.00003894	0.00061750	0.00312083	0.00985752	0.02405940
0.5	0.00004064	0.00064375	0.00325291	0.01027400	0.02507530
0.6	0.00004251	0.00067240	0.00339682	0.01072760	0.02618120
0.7	0.00004459	0.00070386	0.00355435	0.01122360	0.02739000
0.8	0.00004696	0.00073873	0.00372795	0.01176900	0.02871780
0.9	0.00004989	0.00077841	0.00392202	0.01237480	0.03018830

and roller-supported, respectively. The model is tested for different values of (*h/r*).

For the clamped FGP circular plate type, the deflection values obtained for UMCR, SMCR and MMCR material types are presented in Figs. 8, 9, 10, 11 and 12. From the results, an increase in the maximum vertical displacement is observed, in the value of UMCR compared to MMCR and SMCR types, after crossing the porosity coefficient of 0.4. However, it is consistent with the values before this value.

For the roller-supported FGP circular plate, as shown in Figs. 13, 14 and 15, it is observed that the maximum vertical displacement of the MMCR is higher than those of the UMCR before the porosity coefficient of 0.6, while it showed the opposite of its performance, with a decrease in its value and

Table 13 Maximum vertical displacement values of roller-supported MMCR porous circular plate (mm)

	h/r				
e_0	1/10	1/20	1/30	1/40	1/50
0.1	0.00004666	0.00074289	0.00375751	0.01187180	0.02897950
0.2	0.00004857	0.00077333	0.00391146	0.01235820	0.03016680
0.3	0.00005070	0.00080736	0.00408361	0.01290210	0.03149450
0.4	0.00005312	0.00084577	0.00427788	0.01351590	0.03299290
0.5	0.00005586	0.00088957	0.00449945	0.01421600	0.03470180
0.6	0.00005904	0.00094017	0.00475541	0.01502470	0.03667610
0.7	0.00006276	0.00099946	0.00505536	0.01597250	0.03898950
0.8	0.00006720	0.00107022	0.00541333	0.01710360	0.04175070
0.9	0.00007260	0.00115643	0.00584950	0.01848180	0.04511500

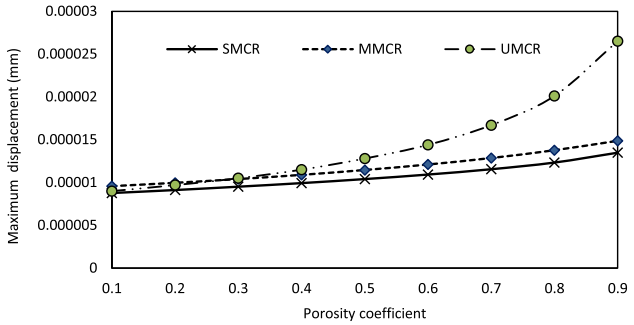


Fig. 3 Comparison of maximum vertical displacements for FGP clamped circular plate ($h/r = 1/10$)

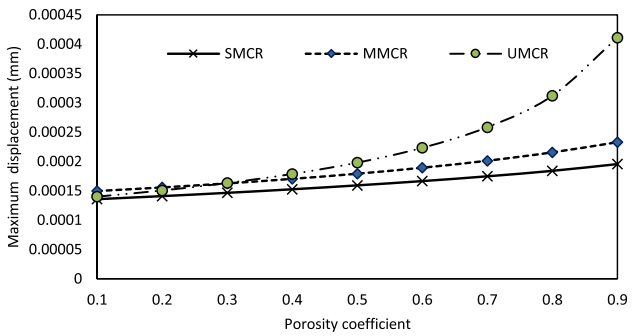


Fig. 4 Comparison of maximum vertical displacements for FGP clamped circular plate ($h/r = 2/10$)

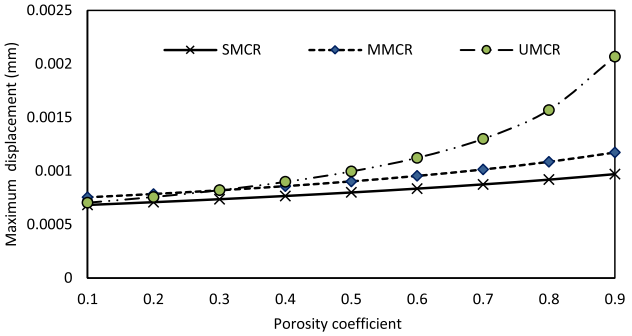


Fig. 5 Comparison of maximum vertical displacements for FGP clamped circular plate ($h/r = 3/10$)

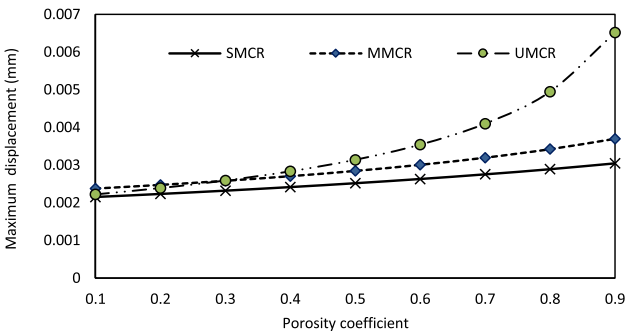


Fig. 6 Comparison of maximum vertical displacements for FGP clamped circular plate ($h/r = 4/10$)

an increase in the value of UMCR type after crossing this the point.

The comparison of modulus of elasticity between SMCR, UMCR, and MMCR porosity material types with porosity coefficients of 0.6 and 0.4 are presented in Figs. 14 and 15. As it can be seen in Figs. 14 and 15, the lowest elasticity is observed in the uniform porosity type, so the highest expected displacement occurs in this type of material. This harmony is achieved in the results.

The comparison between modulus of elasticity of 0.2, 0.4, 0.6 and 0.8 porosity coefficients for uniform porosity material type show that the lowest elasticity value appeared in the 0.8 porosity coefficient. Consequently, the maximum anticipated displacement occurs in this type of material. Therefore, the deflection of the plate increases as the porosity coefficient (e_0) increases.

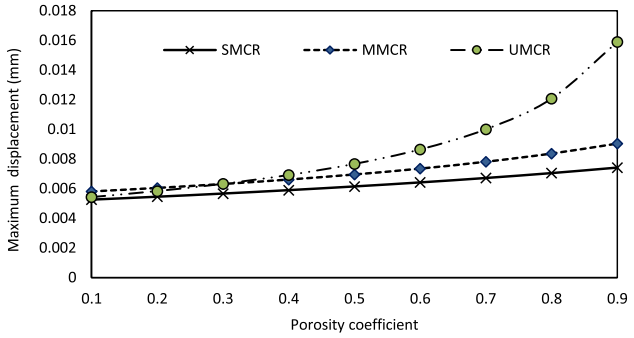


Fig. 7 Comparison of maximum vertical displacements for FGP clamped circular plate ($h/r = 5/10$)

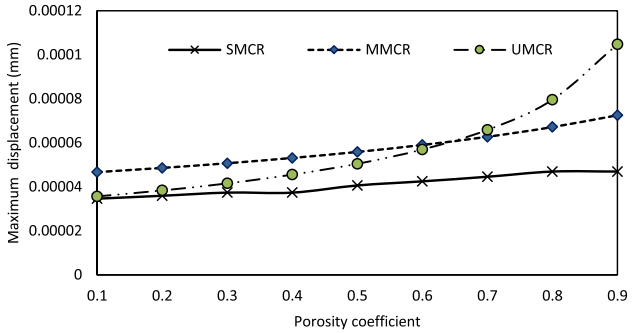


Fig. 8 Comparison of the maximum vertical displacements for FGP roller-support circular plate ($h/r = 1/10$)

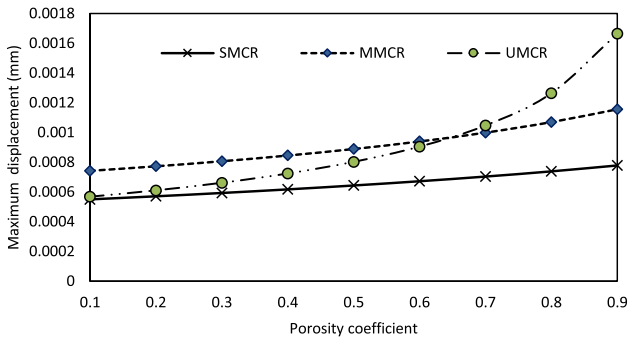


Fig. 9 Comparison of the maximum vertical displacements for FGP roller-support circular plate ($h/r = 2/10$)

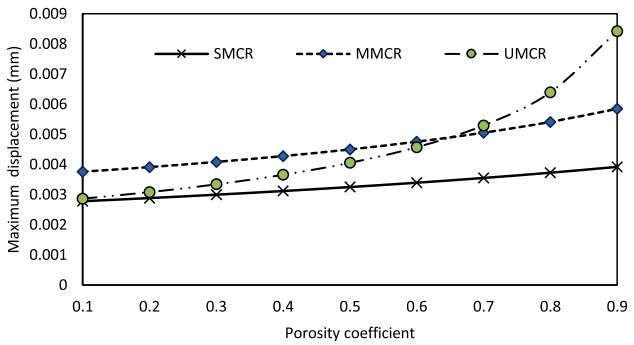


Fig. 10 Comparison of the maximum vertical displacements for FGP roller-support circular plate ($h/r = 3/10$)

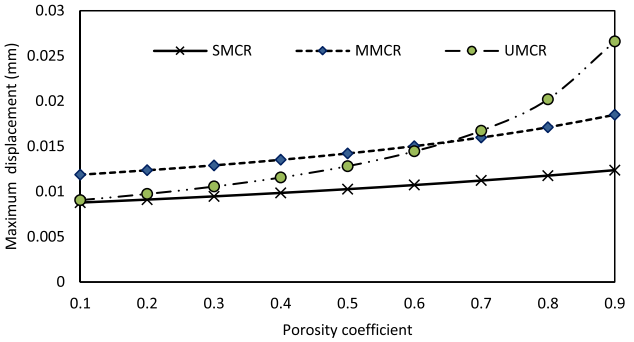


Fig. 11 Comparison of the maximum vertical displacements for FGP roller-support circular plate ($h/r = 4/10$)

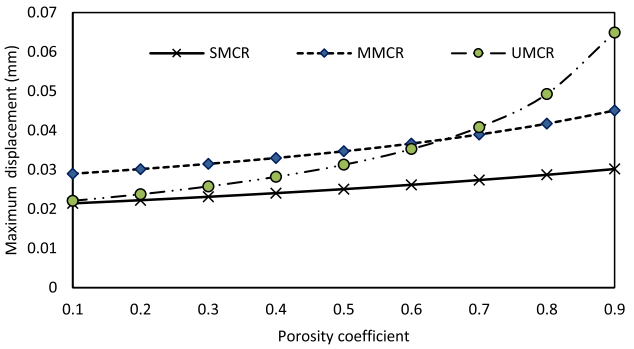


Fig. 12 Comparison of the maximum vertical displacements for FGP roller-support circular plate ($h/r = 5/10$)

4 Conclusion

This paper aims to investigate the axisymmetric bending response of functionally graded porous plates with the aid of the finite element method based on the Galerkin's approach. An eight-node quadrilateral element with two degrees of freedom on each node is implemented in the analysis. The Gauss quadrature is employed for the process of numerical integration. Results of the presented approach are verified with a comparison between the numerical results of (FGM) circular plates and the previous literature, and good agreement is observed. After the validation of the suggested scheme, it is used to investigate the static response of functionally graded porous circular plates for various thickness/radius ratios, porosity coefficients, three different material distributions (UMCR, MMCR, SMCR) and two boundary conditions. Based on the results obtained from the static response of FGP plates, the following important points can be concluded.

- The deflection of the plate increases as the porosity coefficient (e_0) increases.
- The maximum displacement observed in uniform porosity material type is greater than that of other porosity material types for the values of e_0 greater than 0.4 (clamped) and

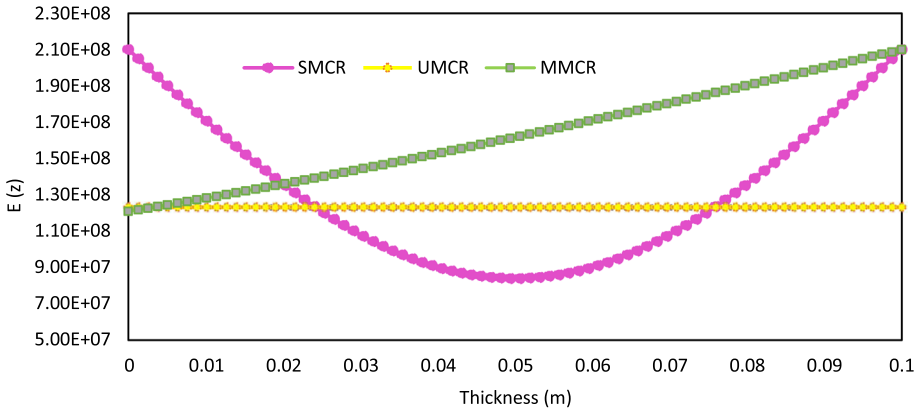


Fig. 13 Comparison of modulus of elasticity between SMCR, UMCR and MMCR types with porosity coefficients of (0.6)

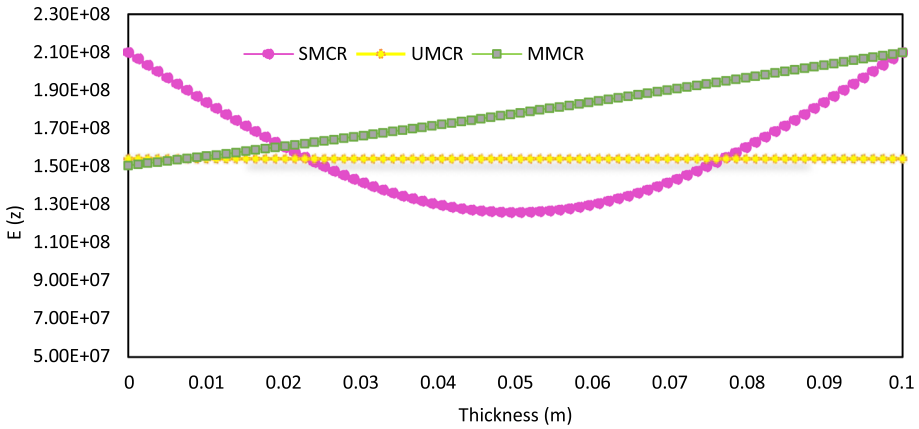


Fig. 14 Comparison of modulus of elasticity between SMCR, UMCR and MMCR types with porosity coefficients of (0.4)

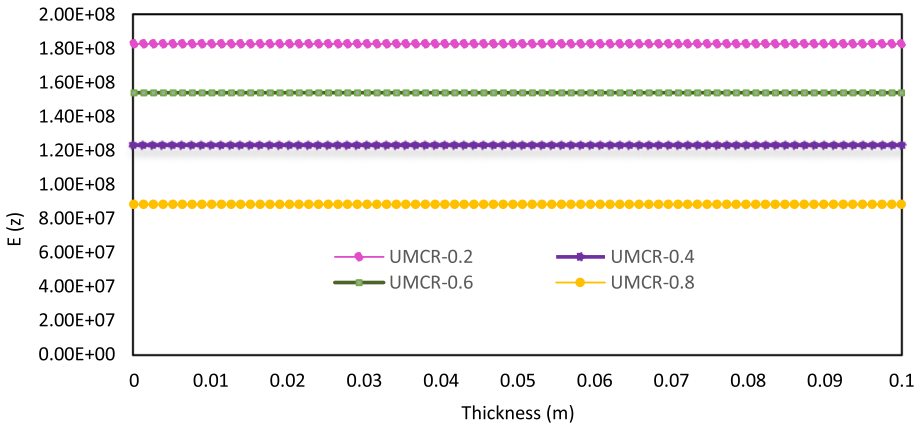


Fig. 15 Comparison between modulus of elasticity of (0.2), (0.4), (0.6) and (0.8) porosity coefficients for uniform porosity material type

0.6 (roller supported). For porosity coefficients less than 0.4 (clamped) and 0.6 (roller supported), the MMCR plates have higher vertical displacements.

- It can be concluded from the results that an increase in the ratio (h/r) leads to an increase in maximum displacement.
- The effect (h/r) on the maximum displacement of the clamped plate is less than on roller-supported FGP plates.
- It is believed that the results of the present study can be used as benchmark solutions for future studies on functionally graded porous circular plates.

Funding Open access funding provided by the Scientific and Technological Research Council of Türkiye (TÜBİTAK).

Open Access This article is licensed under a Creative Commons Attribution 4.0 International License, which permits use, sharing, adaptation, distribution and reproduction in any medium or format, as long as you give appropriate credit to the original author(s) and the source, provide a link to the Creative Commons licence, and indicate if changes were made. The images or other third party material in this article are included in the article's Creative Commons licence, unless indicated otherwise in a credit line to the material. If material is not included in the article's Creative Commons licence and your intended use is not permitted by statutory regulation or exceeds the permitted use, you will

need to obtain permission directly from the copyright holder. To view a copy of this licence, visit http://creativecommons.org/licenses/by/4.0/.

References

1. Kieback, B.; Neubrand, A.; Riedel, H.: Processing techniques for functionally graded materials. Mater. Sci. Eng., A **362**(1–2), 81–106 (2003)
2. Foroutan, M.; Moradi-Dastjerdi, R.; Sotoodeh-Bahreini, R.: Static analysis of FGM cylinders by a mesh-free method. Steel Compos. Struct. **12**(1), 1–11 (2011)
3. Udupa, G.; Rao, S.S.; Gangadharan, K.V.: Functionally graded composite materials: an overview. Procedia Mater. Sci. **5**, 1291–1299 (2014)
4. Kaya, K.; Olmuş, İ; Dördüncü, M.: Investigation of fracture behaviour of one-dimensional functionally graded plates by using peridynamic theory. J. Fac. Eng. Archit. Gazi Univ. **38**(1), 319–329 (2023)
5. Yoo, S.W.; Lee, C.M.; Kim, D.-H.: Effect of functionally graded material (FGM) interlayer in metal additive manufacturing of inconel-stainless bimetallic structure by laser melting deposition (LMD) and wire arc additive manufacturing (WAAM). Materials. **16**(2), 535 (2023)
6. Momennia, S., & Akbarzadeh, A. H. (n.d.): Analysis of functionally graded rectangulare and circular plates using finite element method. In: 16th International Conference on Composite Structures, (2011)
7. Khayal, O.M.E.S.: Delamination phenomenon in composite laminated plates and beams. Bioprocess. Eng. **4**(1), 9–16 (2020)
8. Nguyen, T.H.; Nguyen, T.T.; Tran, T.T.; Pham, Q.H.: Research on the mechanical behaviour of functionally graded porous sandwich plates using a new C1 finite element procedure. Results Eng. **17**, 100817 (2023)
9. Shariyat, M.; Asemi, K.: Three-dimensional non-linear elasticity-based 3D cubic B-spline finite element shear buckling analysis of rectangular orthotropic FGM plates surrounded by elastic foundations. Compos. B Eng. **56**, 934–947 (2014)
10. Al-Itbi, S.K.; Noori, A.R.: Influence of porosity on the free vibration response of sandwich functionally graded porous beams. J. Sustain. Constr. Mater. Technol. **7**(4), 291–301 (2022)
11. Talha, M.; Singh, B.N.: Static response and free vibration analysis of FGM plates using higher order shear deformation theory. Appl. Math. Model. **34**(12), 3991–4011 (2010)
12. Zafarmand, H.; Kadkhodayan, M.: Three-dimensional static analysis of thick functionally graded plates using graded finite element method. Proceedings of the institution of mechanical engineers. J. Mech. Eng. Sci. **228**(8), 1275–1285 (2014)
13. Talha, M.; Singh, B.N.: Stochastic perturbation-based finite element for buckling statistics of FGM plates with uncertain material properties in thermal environments. Compos. Struct. **108**(1), 823–833 (2014)
14. Gilewski, W.; Pełczynski, J.: Material-oriented shape functions for FGM plate finite element formulation. Materials. **13**(3), 803 (2020)
15. Özakça, M.; Tayşi, N.; Kolcu, F.: Buckling analysis and shape optimization of elastic variable thickness circular and annular plates-I. Finite element formulation. Eng. Struct. **25**(2), 181–192 (2003)
16. Nagesh; Gupta, N.K.: Response simulations of clamped circular steel plates under uniform impulse and effects of axisymmetric stiffener configurations. Int. J. Impact Eng. **159**, 104049 (2022)
17. Ma, L.S.; Wang, T.J.: Relationships between axisymmetric bending and buckling solutions of FGM circular plates based on third-order plate theory and classical plate theory. Int. J. Solids Struct. **41**(1), 85–101 (2004)
18. Liu, B.; Ferreira, A.J.M.; Xing, Y.F.; Neves, A.M.A.: Analysis of functionally graded sandwich and laminated shells using a layer-wise theory and a differential quadrature finite element method. Compos. Struct. **136**, 546–553 (2016)
19. Mellouli, H.; Jrad, H.; Wali, M.; Dammak, F.: Meshfree implementation of the double director shell model for FGM shell structures analysis. Eng. Anal. Boundary Elem. **99**, 111–121 (2019)
20. Liew, K.M.; He, X.Q.; Kitipornchai, S.: Finite element method for the feedback control of FGM shells in the frequency domain via piezoelectric sensors and actuators. Comput. Methods Appl. Mech. Eng. **193**(3–5), 257–273 (2004)
21. Chaker, A.; Koubaa, S.; Mars, J.; Vivet, A.; Dammak, F.: An efficient ABAQUS solid shell element implementation for low velocity impact analysis of FGM plates. Eng. Comput. **37**(3), 2145–2157 (2021)
22. Ghomshei, M.M.; Abbasi, V.: Thermal buckling analysis of annular FGM plate having variable thickness under thermal load of arbitrary distribution by finite element method. J. Mech. Sci. Technol. **27**(4), 1031–1039 (2013)
23. Tran, T.T.; Pham, Q.H.; Nguyen-Thoi, T.: An edge-based smoothed finite element for free vibration analysis of functionally graded porous (FGP) plates on elastic foundation taking into mass (EFTIM). Math. Probl. Eng.. **2020**, 1–17 (2020)
24. Li, Q.; Wu, D.; Chen, X.; Liu, L.; Yu, Y.; Gao, W.: Nonlinear vibration and dynamic buckling analyses of sandwich functionally graded porous plate with graphene platelet reinforcement resting on Winkler-Pasternak elastic foundation. Int. J. Mech. Sci. **148**, 596–610 (2018)
25. Pham, Q.H.; Tran, T.T.; Nguyen, P.C.: Dynamic response of functionally graded porous-core sandwich plates subjected to blast load using ES-MITC3 element. Compos. Struct. **309**, 116722 (2023)
26. Turan, M.; Adiyaman, G.: Free vibration and buckling analysis of porous two-directional functionally graded beams using a higher-order finite element model. J. Vib. Eng. Technol. (2023). https://doi.org/10.1007/s42417-023-00898-5
27. Wu, D.; Liu, A.; Huang, Y.; Huang, Y.; Pi, Y.; Gao, W.: Dynamic analysis of functionally graded porous structures through finite element analysis. Eng. Struct. **165**, 287–301 (2018)
28. Shafiei, N.; Mirjavadi, S.S.; MohaselAfshari, B.; Rabby, S.; Kazemi, M.: Vibration of two-dimensional imperfect functionally graded (2D-FG) porous nano-/micro-beams. Comput. Methods Appl. Mech. Eng. **322**, 615–632 (2017)
29. Noori, A.R.; Aslan, T.A.; Temel, B.: Dynamic analysis of functionally graded porous beams using complementary functions method in the Laplace domain. Compos. Struct. **256**, 113094 (2021)
30. Tran, T.T.; Pham, Q.H.; Nguyen-Thoi, T.: Static and free vibration analyses of functionally graded porous variable-thickness plates using an edge-based smoothed finite element method. Defence Technol. **17**(3), 971–986 (2021)
31. Noori, A.R.; Aslan, T.A.; Temel, B.: dairesel plakların sonlu elemanlar yöntemi ile laplace uzayında dinamik analizi. Niğde Ömer Halisdemir Üniversitesi Mühendislik Bilimleri Dergisi. **8**(1), 193–205 (2019). https://doi.org/10.28948/ngumuh.516874
32. Kutlu, A.; Omurtag, M.H.: Large deflection bending analysis of elliptic plates on orthotropic elastic foundation with mixed finite element method. Int. J. Mech. Sci. **65**(1), 64–74 (2012)
33. Jadhav, P.; Bajoria, K.: Stability analysis of piezoelectric FGM plate subjected to electro-mechanical loading using finite element method. Int. J. Appl. Sci. Eng. **11**(4), 375–391 (2013)
34. Temel, B.; Noori, A.R.: A unified solution for the vibration analysis of two-directional functionally graded axisymmetric Mindlin-Reissner plates with variable thickness. Int. J. Mech. Sci. **174**, 105471 (2020)
35. Li, K.; Wu, D.; Gao, W.: Spectral stochastic isogeometric analysis for static response of FGM plate with material uncertainty. Thin-Wall. Struct. **132**, 504–521 (2018)

36. Doori, S.; Noori, A.R.: Finite element approach for the bending analysis of castellated steel beams with various web openings. ALKU J. Sci. **2**(3), 38–49 (2021)
37. Kiarasi, F.; Babaei, M.; Mollaei, S.; Mohammadi, M.; Asemi, K.: Free vibration analysis of FG porous joined truncated conical-cylindrical shell reinforced by graphene platelets. Adv. Nano Res. **11**(4), 361 (2021). https://doi.org/10.12989/anr.2021.11.4.361
38. Kiarasi, F.; Babaei, M.; Asemi, K.; Dimitri, R.; Tornabene, F.: Three-dimensional buckling analysis of functionally graded saturated porous rectangular plates under combined loading conditions. Appl. Sci. **11**(21), 10434 (2021). https://doi.org/10.3390/app112110434
39. Babaei, M.; Kiarasi, F.; Hossaeini Marashi, S.M.; Ebadati, M.; Masoumi, F.; Asemi, K.: Stress wave propagation and natural frequency analysis of functionally graded graphene platelet-reinforced porous joined conical–cylindrical–conical shell. Waves Random Complex Media (2021). https://doi.org/10.1080/17455030.2021.2003478
40. Babaei, M.; Kiarasi, F.; Asemi, K.; Dimitri, R.; Tornabene, F.: Transient thermal stresses in FG porous rotating truncated cones reinforced by graphene platelets. Appl. Sci. **12**(8), 3932 (2022). https://doi.org/10.3390/app12083932
41. Babaei, M.; Asemi, K.: Stress analysis of functionally graded saturated porous rotating thick truncated cone. Mech. Based Des. Struct. Mach. **50**(5), 1537–1564 (2022). https://doi.org/10.1080/15397734.2020.1753536
42. Khatounabadi, M.; Jafari, M.; Asemi, K.: Low-velocity impact analysis of functionally graded porous circular plate reinforced with graphene platelets. Waves Random Complex Media (2022). https://doi.org/10.1080/17455030.2022.2091182
43. Asemi, K.; Babaei, M.; Kiarasi, F.: Static, natural frequency and dynamic analyses of functionally graded porous annular sector plates reinforced by graphene platelets. Mech. Based Des. Struct. Mach. **50**(11), 3853–3881 (2022). https://doi.org/10.1080/15397734.2020.1822865
44. Xia, L.; Wang, R.; Chen, G.; Asemi, K.; Tounsi, A.: The finite element method for dynamics of FG porous truncated conical panels reinforced with graphene platelets based on the 3-D elasticity. Adv. Nano. Res. **14**(4), 375–389 (2023). https://doi.org/10.12989/anr.2023.14.4.375
45. Zhou, Z.; Wang, Y.; Zhang, S.; Dimitri, R.; Tornabene, F.; Asemi, K.: Numerical study on the buckling behavior of fg porous spherical caps reinforced by graphene platelets. Nanomaterials **13**(7), 1205 (2023). https://doi.org/10.3390/nano13071205
46. Babaei, M.; Kiarasi, F.; Asemi, K.: Torsional buckling response of FG porous thick truncated conical shell panels reinforced by GPLs supporting on Winkler elastic foundation. Mech. Based Design Struct. Mach. (2023). https://doi.org/10.1080/15397734.2023.2205488
47. Chandrupatla, T.; Belegundu, A.: Introduction to finite elements in engineering (Book). Cambridge University Press, Cambridge (2021)
48. Wattanasakulpong, N.; Eiadtrong, S.: Transient responses of sandwich plates with a functionally graded porous core: Jacobi-Ritz method. Int. J. Struct. Stab. Dyn. **23**(04), 2350039 (2023)
49. Dhatt, G.; Touzot, G.: The finite element method displayed (Book), 1st edn. Kluwer, Wiley, Hoboken (1984)
50. Saidi, A.R.; Rasouli, A.; Sahraee, S.: Axisymmetric bending and buckling analysis of thick functionally graded circular plates using unconstrained third-order shear deformation plate theory. Compos. Struct. **2009**(89), 110–119 (2009)
51. Reddy, J.N.; Wang, C.M.; Kitipornchai, S.: Axisymmetric bending of functionally graded circular and annular plates. Eur. J. Mech. -A/Solid **18**, 185–199 (1999)
52. Noori, A.R.; Temel, B.: A powerful numerical approach for the axisymmetric bending response of shear deformable two-directional functionally graded (2D-FG) plates with variable thickness. Proc. Inst. Mech. Eng. C J. Mech. Eng. Sci. **235**(22), 6370–6387 (2021)
53. Mechanical APDL element reference. Canonsburg, PA, (2013)